Rakenteiden Mekaniikka (Journal of Structural Mechanics)
Vol. 57, No. 1, 2024, pp. 1–23
http://rakenteidenmekaniikka.journal.fi
https://doi.org/10.23998/rm.137617

VERTAISARVIOITU
KOLLEGIALT GRANSKAD
PEER-REVIEWED
www.tsv.fi/tunnus

Behavior of fin-plate connection of a composite beam subjected to different fire scenarios

Mohamed Sakr, Wei Lu[1], Ivar Talvik and Jari Puttonen

Summary The behavior of fin-plate connections of a composite beam exposed to different fire scenarios was numerically studied by experimentally validated models. At elevated temperatures, the closure of the gap between the beam end and column was observed to transform a hinge connection to a moment connection, reducing the beam deflection. In fire, a slow cooling of the beam close to the connection is a favourable approach to affect the responses of the beam and the fin-plate connection. Under heating and cooling cycles, the axial forces developed in the beam fluctuated between compression and tension. At the end of the first cooling phase, the shear plate was found to be a critical member in which the further development of the axial tension force can fracture the fin-plate connection at the end of the second cooling phase.

Key words: simple shear connections, composite beams, traveling fires, heating and cooling cycles

Received: 2 October 2023. Accepted: 30 January 2024. Published online: 27 March 2024.

Introduction

The increased use of steel and concrete composite structures in construction industry has improved the structural durability and structural integrity, lowered the labour costs, and accelerated project schedules. By applying environmentally friendly design strategies to determine the proportions of the material components in the composite members [1], carbon dioxide emissions can be effectively reduced. However, fire poses an ongoing risk to the structural safety of steel members and joints. Fire scenario is one of the main factors affecting the disproportionate collapse of composite structures. The structural members exposed to different fire scenarios behave differently. Furthermore, structural details as connections can be even more important for the fire safety of building than the global response of structural members.

[1] Corresponding author: wei.2.lu@aalto.fi

The impact of fire scenarios depends on the size of compartments and the heating location of the fire regarding the location of the member. It is reasonable to assume uniform heating in a small-size compartment. However, in the large size compartment, the fires can stay locally or travel across the floor, invaliding the assumptions of uniform heating. Large scale fire tests have pointed out that a temperature field with a significant non-uniformity along the length, the width, and the height of the compartment may exist [2]. Along the span of the composite beams, the non-uniform temperature field can be caused by localized fire or travelling fire.

The fire curves produced by the travelling fire models often include one peak. However, the double peaks of adiabatic surface temperatures at ceilings for different ventilation conditions were reported by Ramsamy et al. [3]. The second peak has not been predicted by the travelling fire methodology that is currently available. Besides the double peaks, the temperature–time profiles also had multiple local peaks. Very often, these local peaks were treated as noises and the fire curves were smoothened for thermal and mechanical analyses. However, these local heating-cooling cycles or double peaks in travelling fire may influence on the structural response and material properties.

Less research is available on studying the behaviour of structural elements and connections under the heating and cooling cycles. The studies in [4] revealed that the frames under irregular fluctuations of the axial forces and bending moments were because different bays were cooled at different times. Shakil et. al [5] revealed that the beams within elastic range are prone to the fluctuations of the axial force. The fluctuations are mainly caused by non-uniform temperature field along the beam exposed to the travelling fire with multiple peaks. At higher load ratios, the plastification of the material cushioned the fluctuations in the axial force response. During the heating and cooling cycles, if the beams are unloaded from plastic range to elastic range, the accumulation of the residual deformations can activate the catenary actions at temperatures below 400 °C. The similar fluctuations of the structural responses of the steel truss beams inside the warehouse with and without fire interventions were also reported in [6] and [7] because of the heating and cooling cycles during the fire spreading and backward travelling and during the cooling by insufficient water sprays. In these studies, the connections between steel beams and columns were modelled either as pinned connections or fixed connections without considering connection details. In addition, the composite actions between the steel beams and concrete slabs were not modelled. The studies in [8–12] have shown that the structural response of composite beams with simple shear connections are different from those of the studied steel beams because of the different temperature distributions and loading conditions. Over the sections of composite beams, the concrete slab supported by steel beams may create a non-uniform temperature field in fire. However, the non-uniformity along the span has not been considered. Therefore, the objective of this research is to study the behaviour of simple fin plate connections of composite beams exposed to different heating and cooling conditions at different locations along the span especially the heating and cooling cycles observed in travelling fires or in fire interventions.

The outline of the paper is as follows. The 3D FE models of both thermal and mechanical analyses were created for the composite beams with shear tab connections. The FE models were validated by the temperatures and deflections reported in the tests [10, 11]. The validated models were used to study the load-bearing mechanism of the

composite beams and failure mechanism of shear tab connections. Based on these mechanisms, the effects of the following parameters on the behaviour of the composite beam and its fin plate connections are studied: gap width between the beam end and the column, location of fire on the beam span, cooling rate, and fire scenario.

FE models for thermal and mechanical analyses

Benchmark tests

To examine the behaviour of simple connections between composite beams and column in fire, two benchmark tests (CB-3 and CB-4) performed at Purdue University [17] were selected for creating FE models. The test setup and the specimen details are shown in Figure 1 and Figure 2. A composite beam was connected to two steel columns using shear tab connections. In one test (CB-3), a load of 156 kN (60% of its load-carrying capacity at room temperature) was first applied to the mid-span of the beam (Figure 1 (a)), and then the beam was heated using high-temperature ceramic fibre heaters as shown in Figure 1 (b). The heaters were individually controlled, allowing different heating rates for the concrete and steel surfaces of the composite beam. In the other test (CB-4), the beam was loaded and heated similarly but with a load value of 111 kN and a maximum temperature of 700℃. [11]

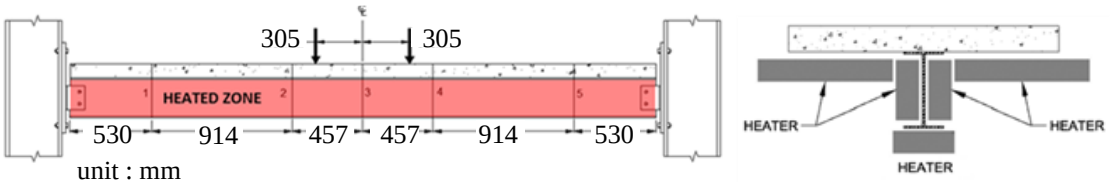

(a) (b)

Figure 1. Benchmark tests (a) loading and heating configurations (b) locations of heaters. [11]

Figure 2 presents the details of the beam and the connections. The composite beam was a W10 × 22 steel beam topped by an 88.9 mm thick and 914 mm wide concrete slab. The concrete slab and the top flange of the steel beam were connected by 13 mm diameter shear studs spaced at intervals of 152 mm along the center line of the beam. A 6 × 6 W2.0 × 2.0 wire mesh reinforcement was used in the slab with a cover of 19 mm to provide a fire-resistance rating of two hours. The composite beam was connected to the columns (W14 x 109) through fin plate connections, as shown in Figure 2 (b). The column was protected with Fire Resistant Cement Spraying Material (SFRM) for reaching the same fire rating. The connections were deployed using sacrifice plates so that the columns were reusable for other tests. The sacrificial plate with a thickness of 25 mm was bolted to the column flange. A 6.35 mm thick plate was bolted to the beam with two 19 mm diameter bolts and welded to the sacrificial plate using 7.9 mm welds. The bolts were ASTM A325. Both the composite beam and the connection were designed in accordance with US design practice and AISC specifications. The composite beam was designed to be stronger than the beam-to-column connections. [11]

For both specimens, the failure of the composite beams was checked according to two criteria given in [13], i.e., either following the deflection criterion of $L/20$ or

following both the deflection criterion of L⁄30 and the deformation rate criterion of L^2⁄9000d, in which L is the span of beams and d is the height of beams. The failure of the shear studs was assumed to occur when the slip at elevated temperature reached the value corresponding to the maximum load at room temperature. The welds of the shear tab plate fractured in the end of the cooling phase, leading to the failure of the connection. [11]

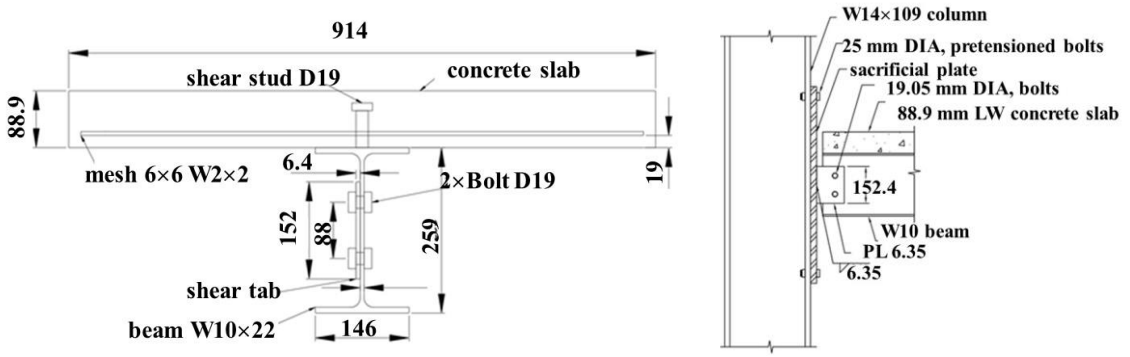

(a) (b)

Figure 2. Details of the specimen (a) dimensions of the cross-section (b) connection details. [11]

FE models created for thermal analyses

The thermal analysis was performed using Abaqus/Standard [14]. A 3D FE model shown in Figure 3 was created for the composite beam connected to the testing frame with fin-plate connections. All parts of the test specimen were modelled using 8-node linear heat transfer brick elements (DC3D8) except the shear studs and reinforcing mesh that were modelled as 2D truss elements (DC1D2). The model consists of 33446 nodes and 21245 elements with a mesh size ranged to 5–50 mm. The mesh was finer close to the connections. Two layers of elements were used through the thickness of the web and the flanges of the steel beam, the concrete slab, and the fin plate. The same mesh size was used at the contact surfaces between the steel beam section and the concrete slab. The density, temperature-dependent thermal conductivity, and specific heat of steel elements such as column, beam, bolts, shear stud, and reinforcing bars were defined according to EN 1993-1-2 [15]. The density, temperature-dependent thermal conductivity and specific heat of concrete slab (C30) were defined according to EN 1992-1-2 [16].

Four types of the thermal boundary conditions were studied, and the details are listed in Table 1. In Case 3, the heating and cooling temperatures of the exposed surfaces of the composite beam were defined as in specimen CB-3 (Figure 1 (b)). The reference temperature of the unexposed surface was defined as 20 °C. In Case 2, the same surface temperatures were defined as in Case 3 except for the surfaces of the top flange. At these surfaces, no heat exchange was assumed so that the effects of the temperatures on the behaviour of shear stud could be investigated. In Cases 1 and 4, the heat flux was defined by using both convection and radiation heat transfer.

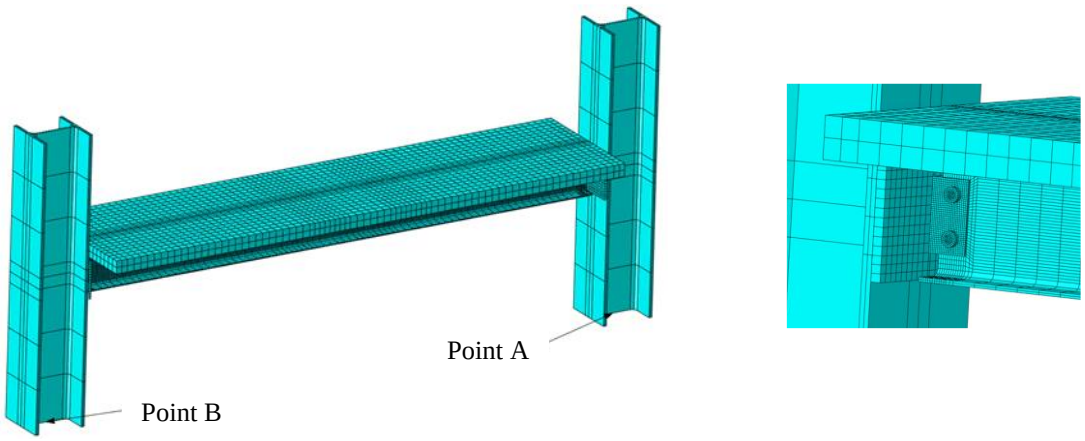

(a) (b)

Figure 3. Three-dimensional FE-models for the tested frame (a) overall view (b) close view of the connection.

Table 1. Studied cases and their heating conditions.

Cases	Thermal input	Max. temperature [°C]
Case 1	heat flux	600
Case 2	no heat exchange on the unexposed surface of the top flange	600
Case 3	surface temperatures as in the test	600
Case 4	heat flux	700

The input gas temperatures are shown in Figure 4 (b). The maximum temperature in Case 1 was 600°C as in the test of CB-3 and in Case 4 was 700°C as in the test of CB-4. The convection coefficient on the exposed surfaces and unexposed surfaces was given as 25 W/m^{2}K and 9 W/m^{2}K, respectively; and the emissivity coefficient was given as 0.7 as given in [15]. Between parts of connections, i.e., bolts, plates, and beam, and between the top flange and the concrete slab, thermal contacts were defined using an option of high conductivity to allow the heat transfer. During the heating and cooling phases, the columns were exposed to the room temperature.

FE models created for mechanical analyses

The mechanical analyses were performed by using the Abaqus/Explicit dynamic procedure [14]. As in the model shown in Figure 3, all parts of the structural frame were modelled using solid elements (C3D8R) with reduced integration and hourglass control except the shear studs were modelled using 2D beam elements (B31) and the reinforcing mesh was modelled using 2D truss elements (T3D2). The model consisted of 33446 nodes and 21245 elements with a mesh size ranging from 5 mm to 50 mm.

The clamped boundary condition was applied to the bottom of columns at the reference points (point A and point B in Figure 3 (a)). To prevent the frame rotation about the longitudinal axis of the beam, the out-of-plane deflection of the top flange was

prevented at the mid-span of the steel beam on both sides similarly as in the test. The shear studs were tied to the top surface of the steel beam using zero-length connector elements. Inside the concrete slab, the embedded constraint was used to simulate the interaction among a shear stud, reinforcing mesh, and the concrete slab. The welds between the shear plate and the sacrificial plate, and between the sacrificial plate and the column were simulated by tie constraints. General contact in Abaqus was defined for all the contact surfaces of connection parts, i.e., bolts, plates, and beam, and between the beam and the concrete slab. A penalty friction coefficient of 0.35 for tangential behavior and hard contact allowing the contact separation were used. The general contacts were defined in all the steps of the simulations.

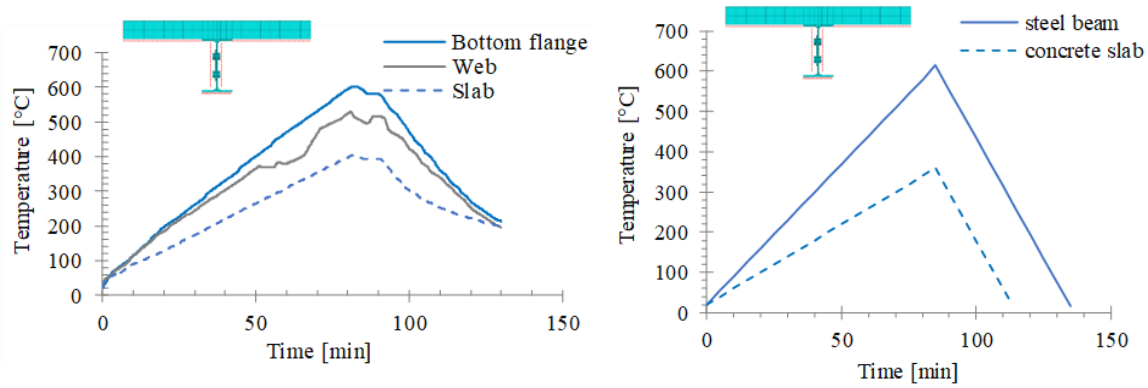

(a) (b)

Figure 4. Thermal boundary conditions (a) surface temperatures for Case 2 and Case 3 (b) gas temperatures for Case 1.

Mechanical properties such as density, temperature-dependent isotropic elasticity, temperature-dependent coefficient of thermal expansion and temperature-dependent plasticity were defined according to [15] and [16] for steel and reinforced concrete, respectively. Since the material properties at elevated temperatures have not been provided in [11], the nominal material properties were used in FE models. Steel beams and plates were modelled with a yield strength of 355 N/mm^2. Bolts were modelled as grade 8.8 with a yield strength of 640 N/mm^2. Reinforcement mesh was modelled as A500 with a yield strength of 500 N/mm^2. The concrete was modelled as C30/37 with a compressive strength of 30 N/mm^2 and a tensile strength of 2.9 N/mm^2. The concrete section was assumed to crack at zero stress under tension. The elastic modulus for structural steel was 210 000 N/mm^2, for steel reinforcement 200 000 N/mm^2, and for concrete 33 000 N/mm^2. The density was 7850 kg/m^3 for steel and 2300 kg/m^3 for concrete. The thermal elongations of steel and concrete were also defined according to [15] and [16], respectively. The properties of the connector element were defined as temperature dependent force-slip functions as in [8].

Analysis procedure

The analysis was performed in two steps. In the first step, the mechanical loading was applied for 30 sec and kept as a constant thereafter. As in the test, two transverse loads

with a value of 156 kN were modelled as a pressure of 3.5 N/mm^2 at two surfaces (152x146 mm) on the top of concrete slab. In the second step, the beam was heated and cooled for 7800 sec (130 min) according to the previously defined thermal conditions. The total simulation time was scaled using mass scaling that was set to 2×10^4 for the loading phase and 1.6×10^6 for the heating and cooling phases.

Validations of FE models and load-bearing mechanism

Validation of FE models for both thermal and mechanical analyses

Figure 6 shows the comparisons of temperatures between FE analysis and test results at selected points of the cross-section at mid-span. In the tests, the thermal couples were installed on the test specimen between Points 1 and 3 in the steel beam and between Points 4 and 5 in the slab. In FE models, the temperatures were extracted along the dashed red lines.

In Case 3, at the points studied, the temperature profiles from FE analyses and those measured from the test matched well when the bottom flange of the steel beam reached 600°C. The thermal FE model was validated for the further studies. In Case 1, when the heat flux was used as input, the temperature of the web close to the top flange was underestimated around 150°C and the temperature of the web close to the bottom flange was overestimated around 50°C. In Case 2, if the heat transfer on the bottom surface of the top flange was not allowed, the temperature on the top flange was overestimated up to 200°C but the temperatures at other locations were not affected. Since the models for both cases reasonably predicted the trend of the temperature profiles, the corresponding temperature history for each case will be used as input for the further mechanical analyses.

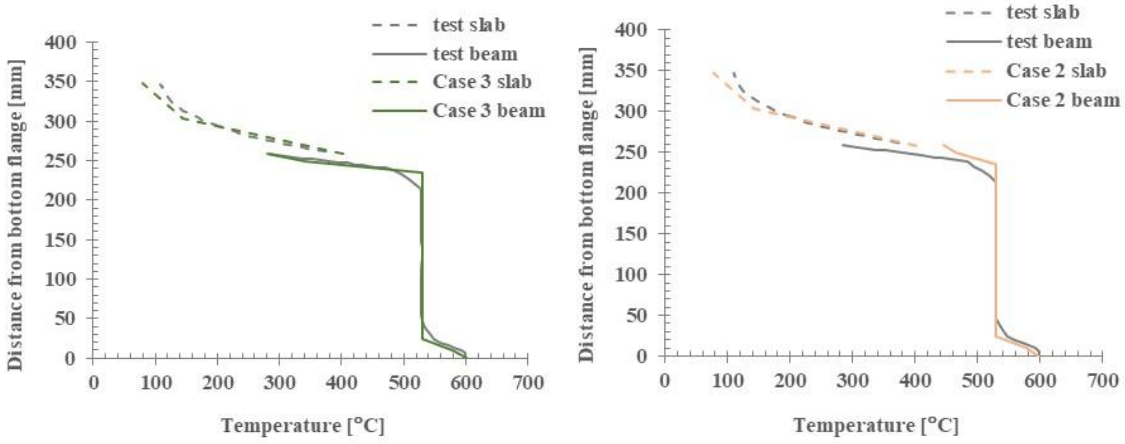

(a) (b)

Figure 6. Comparisons of the temperatures between FE and test results at the selected points when the bottom flange of steel beam reached 600°C (a) Case 3 (b) Case 2 (c) Case 1 (d) selected points 1 to 5 at mid-span of the beam [11].

Figure 7 (a) and (b) compare the vertical displacements between FE and test results at both mid-span and quarter span, respectively. The midspan displacements predicted by the FE models and those measured in the test had a similar trend. In the heating

phase, FE results differ from test values after 200℃. When the bottom surface of the bottom flange reached 600℃, the FE predictions were about 6% to 13% higher than the test results. In the cooling phase, the deflections received from FE analyses and the test results match well between 600℃ and 400℃. The deviation from the test results was up to 18% when the bottom flange reached the temperature of 200°C. As for the displacements, the results at the quarter-span had similar differences between FE and test results in both heating and cooling phases. The match between FE and test results reasonably validated the FE models.

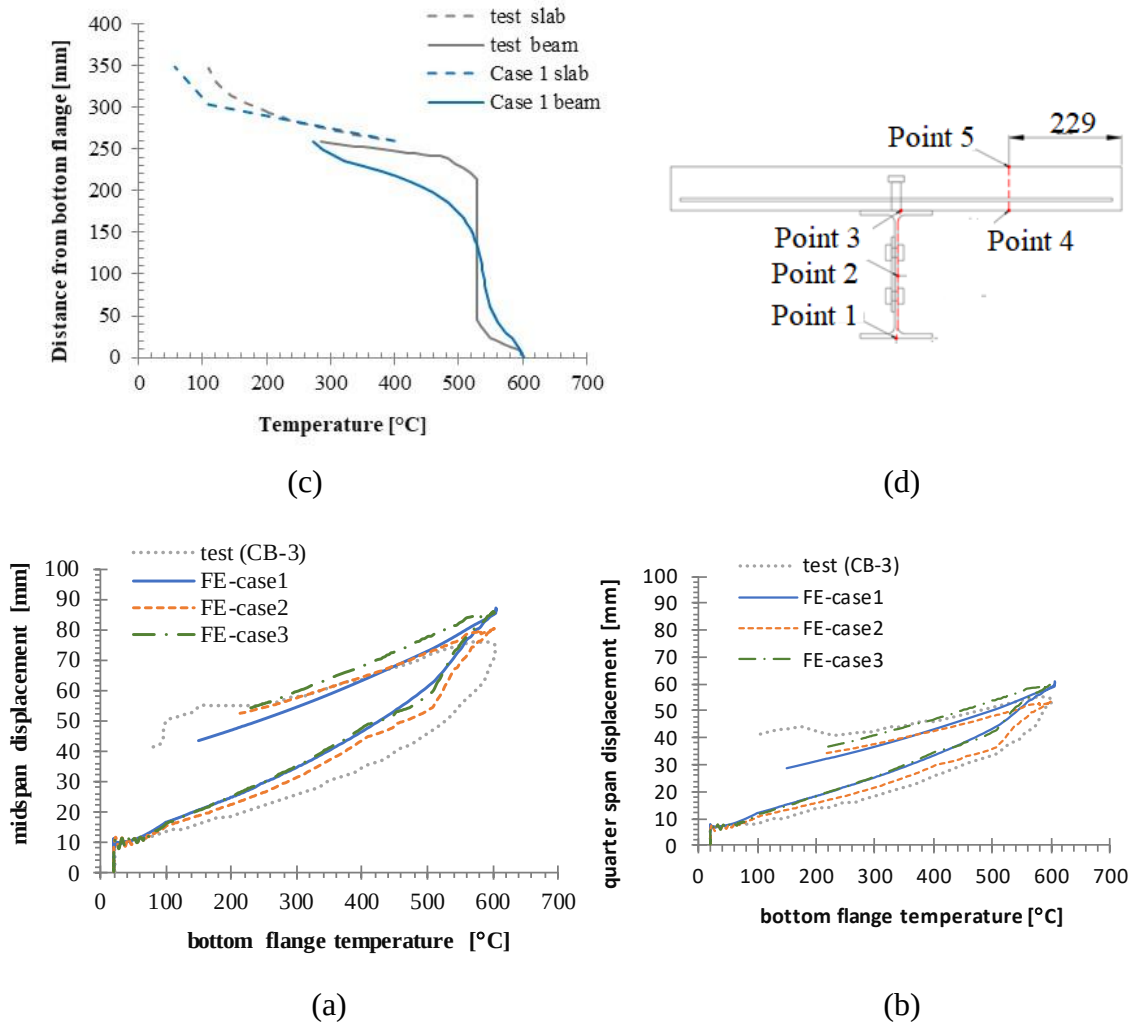

Figure 7. Displacement – temperature curves measured at the bottom flange of the cross-section at (a) mid-span (b) quarter span from both FE analyses and the test (CB-3) [16].

Figure 8 (a) shows the axial forces developed for all the studied beams. During the heating phase, the maximum axial compression load was less than that reported in [11]. The axial forces were not measured during the tests and the values reported were from the simulations. The differences of axial loads can be a consequence of more non-uniform temperatures along the span of the beam in the tests than in FE analyses. During the cooling phase, the axial forces from FE analyses and the values from the test matched well.

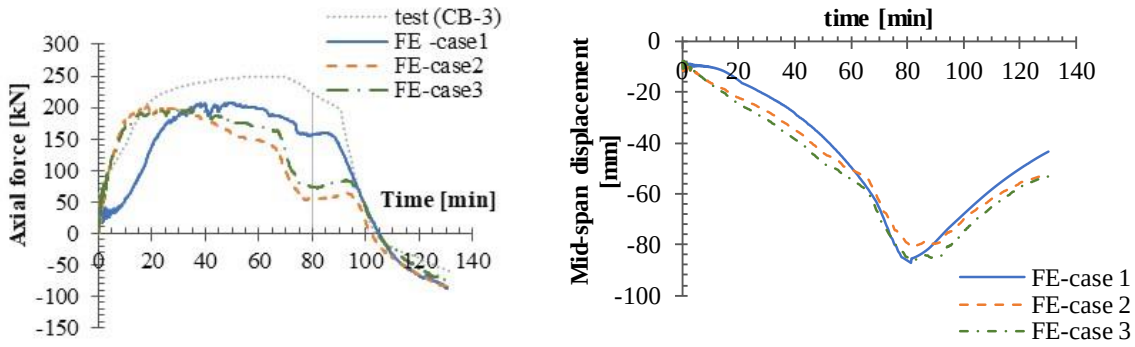

(a) (b)

Figure 8. Comparisons of beam responses among Cases 1 to 3 (a) axial force developed at connections (b) displacement – time curves measured at mid-span.

Load-bearing mechanism of the composite beam

Based on the axial force output at connections, the load-bearing mechanism of the composite beam can be divided into the four stages as with the steel beam. The four stages are explained according to the points marked on the curve output from Case 1 (Figure 8 (a)).

- Stage I (0-1): Development of compression forces. Because of the restrained thermal expansion, the axially compressed force increased linearly with the rise of the temperatures. The first stage ended until the degradation of the elastic modulus of the steel started at around 21 min.
- Stage II (1-3): Transition from compression-controlled to bending-controlled behaviour. As the temperature rose, the material degraded further. The increase of the axial force became non-linear. When the temperature of the bottom flange reached 335°C at around 42 min, the compressive force reached its maximum value of 207 kN. Thereafter, the compressive axial force decreased slowly until point 3 was reached.
- Stage III (3-4): Activation of the tension-controlled behaviour. At point 3, a sudden decrease of the axial compression force was observed. A change of deflection rate was noticed between 65 min and 80 min as shown in Figure 8 (b). The tension force was activated. When the cooling phase started, the axial force remained unchanged until the further decrease of the compressive axial force started at point 4.
- Stage IV (4-5): Development of the catenary action. The controlled cooling forced the beam to convert from compression to tension, thus leading the beam to act as a catenary.

Compared to the beam in Case 3, the beams in Case 2 and Case 1 behaved differently mainly in Stage 2 and Stage 3. In Case 2, the maximum temperatures developed in the web and the top flange is higher than in the other two cases. The higher temperatures degraded the material properties more, leading to a larger deflection. In Case 1, the temperatures of the web and the flange rose gradually, leading to gradually increasing axial forces. Since the web temperatures of the steel beam were lower than

those of the steel beam in Case 2 and Case 3, the axial force in Case 1 reduced less. As shown in Figure 9, the similar four-stage mechanism was also observed in Case 4. Because of the smaller applied load, the beam in Case 4 had a longer fire resistance.

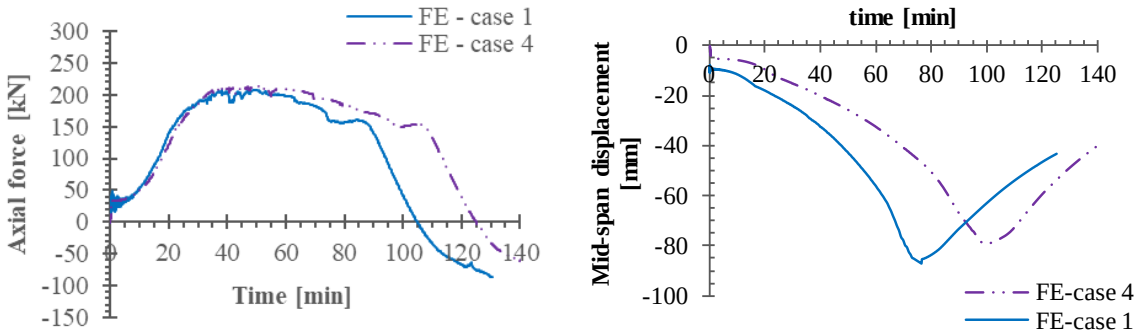

(a) (b)

Figure 9. Comparisons of beam responses between Case 1 and Case 4 (a) axial force developed at connections (b) displacement – time curves measured at mid-span.

The deflection versus time curve correlates well to the five points on the curve of the axially developed force. The material degradation and the hinge mechanism accelerated the deflection. During the cooling stage, both the developed tension force and the material retention recover the deflection. However, the residual deflections are large at the end of the cooling stage. In all the studied cases, the maximum deflection of the composite beams did not exceed the limit of the deflection and of the deflection rate. In general, FE model predict the load transferring mechanism reasonably.

Behavior of shear connectors

The slip of the shear stud located at beam end (Figure 10 (a)) correlates well with four-stage mechanism. The different slip of the shear stud between Cases 1 to 4 are visible in Stages 2 to 4. In Stage 2, the slip of the shear stud changed in a faster rate for all the studied cases. The sudden change of the slip was due to the stiffness degradation of the shear stud when the temperature rose from 100°C to 200°C between 40 min and 75 min (Figure 10 (b)). In Stage 3, the slip initially increased sharply due to the strength degradation at 300°C (Case 1) or changed the slip direction due to the degradation of concrete strength at 400°C (Case 2). The slip of the shear stud then changed directions due to the non-uniform heating across the cross-section of the beam. In Stage 4, the direction of the slip changed due to the restrained thermal contraction.

In Case 2, when the temperature of shear studs reached around 300°C, the slip of the shear studs was about 8 mm, which is larger than 6 mm corresponding to the maximum load at room temperature. According to the criteria defined in [8], the shear studs failed. For other cases, no failures occurred in the shear stud connectors.

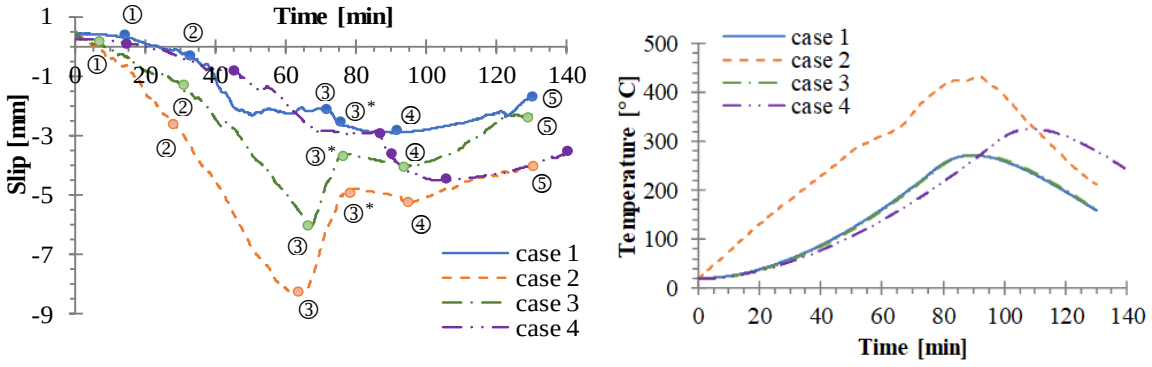

(a) (b)

Figure 10. Temperature and slip development of the shear stud at the beam end (a) slip–time curve (b) temperature–time curve.

Behavior of shear tab connections

In the tests, the shear tab connections failed along the weld line. In the FE model, the weld was modelled as tie constraints, therefore no fracture can be observed. To define the failure in the shear plate, the development of maximum principal stresses inside the beam-to-column connections were studied. Figure 11 shows the distributions of absolute principal stresses of the shear plate at the end of cooling phase for Case 3 and Case 4. The highly tensioned region of the shear plate located at the upper corner close to the welds whereas a highly compressed region located at the lower corner close to welds and near the bolt holes. The highly stressed regions close to welds coincided well with the fracture region reported in the tests for both Case 3 and Case 4. Therefore, the failure of the shear tab connection can be predicted by the maximum principal stresses of the welds close to the upper corner of the tab plate.

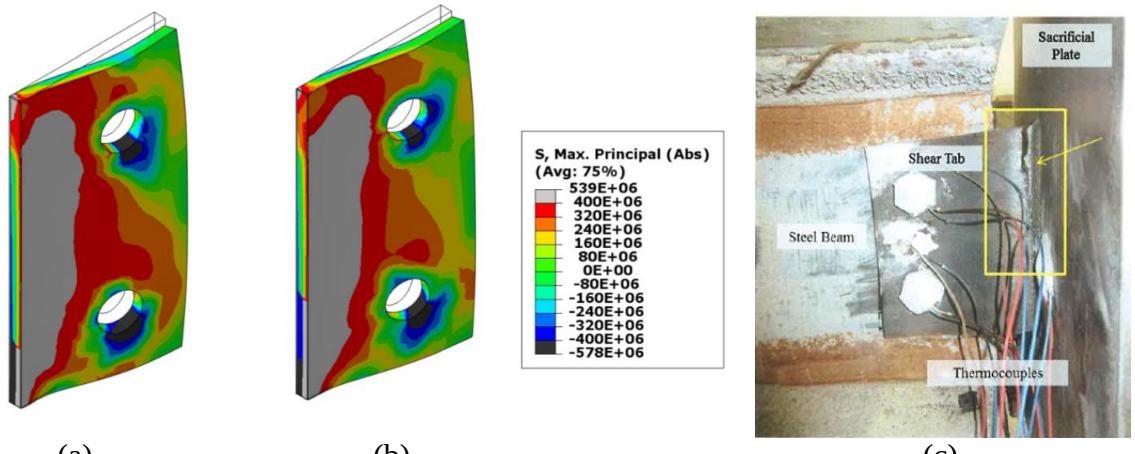

(a) (b) (c)

Figure 11. Comparisons of the maximum principal stress of shear plate from FE results with the fracture of the welds in the test at the end of the cooling phase: (a) Case 3, (b) Case 4, (c) test result [11].

Effects of different fire scenarios on behavior of composite beams and their shear tab connections

The response of the composite beam and the behavior of the shear tab connections were studied by heating and cooling the composite beam at different locations with various fire scenarios. For all the studied cases in this section, the FE models were created using the dimensions of the CB-3 specimen tested. The beam is vertically loaded by 156 kN and the gap between the beam and the connection was 8 mm, which differs from 20 mm used in Cases 1 to 4.

The beam was heated and cooled by the surface temperatures or gas temperatures. The heating rate used was as in the test, but the cooling rate was varied. During the heating and cooling cycles, gas temperatures were used. The surface cooling or the gas cooling was intended to simulate the two cooling scenarios where either the structural member is cooled directly or the fire itself is cooled directly. A cooling rate of 40°C/min was selected as used in [17] for cooling the tensile coupon of S900 in air. The cyclic heating and cooling condition can occur in the travelling fire scenarios as reported in [5] or in applying the water sprays to the beam as reported in [6]. Along the beam span, three heating locations were used: the whole beam, 1 m zone from the connection, and 1 m zone at the middle span of the beam. The variations of the fire scenarios and fire locations are summarized in Table 2.

Table 2. Summary of the studied cases considering fire scenarios and heating locations.

Cases	Duration [min]	Fire scenarios as in the tests	Heating location	Max. temp [°C]	Gap [mm]
Case 3	130	surface temperature	beam	600	20
Case 5	130	surface temperature	beam	600	8
Case 6	150	heating and cooling as in test	beam	600	8
Case 7	150	heating and cooling as in test	1m to connection	600	8
Case 8	110	with faster cooling rate	beam	600	8
Case 9	110	with faster cooling rate	1m to connection	600	8
Case 10	60	cyclic heating and cooling	beam	700	8
Case 11	60	cyclic heating and cooling	1m to connection	700	8
Case 12	60	cyclic heating and cooling	1m at the center	700	8

Response of composite beams with different parameters

Effects of the gap distance

Two values of the gap distances were considered in the FE models: 20 mm (Case 3) and 8 mm (Case 5), as shown in Figure 14 (a). The beams were heated by surface temperatures as in the test. The axial forces developed at the ends of the beams were output from both shear plate and sacrifice plate, and the results are compared in Figure 15. The rotation of the beam could close the gap and create contact between the beam ends and the sacrificing plate, changing the response of the beam.

In Case 3, the gap distance of 20 mm allowed the rotations of the beam and delayed the closure of the gap till around 75 min (Figure 12 (b)). The compression forces at sacrificial plate and shear plate were the same until large rotation occurred in Stage III. The contacts increased the axial force at sacrificial plate approximately 40% more than at shear plate.

In Case 5, the compression forces were quite like those in Case 3 during the heating phase until the gap was closed at 32 min. The smaller gap of 8 mm in Case 5 increased the axial forces rapidly in the sacrificial plate as the beam was pushing against the column. Compression forces reached 575 kN at 68 min. Due to the additional restraints to the beam from the closure of the gap in Case 5, the transition of forces from compression to tension forces was delayed about 7 minutes. At the end of the cooling stage, the tension was equally developed in both cases.

In addition, in both cases, the beam with a gap of 8 mm followed the benchmark test more closely in Stage III, where in Stage IV, the behavior of the beam with a gap of 20 mm was closer to the benchmark test. Therefore, the actual gap used in the tests was between 8 mm and 20 mm. The gap of 8 mm was selected for the parametric studies.

The consistency of the displacements between Case 3 and Case 5 was observed in Figure 13 (b). The displacements of Case 5 and Case 3 matched well till the contacts were established between the beam and the sacrificial plate. The maximum displacement at the mid-span was 57 mm in Case 5 and 81 mm in Case 3. The reduced displacement in Case 5 was because the contact changed a hinged connection to a moment connection.

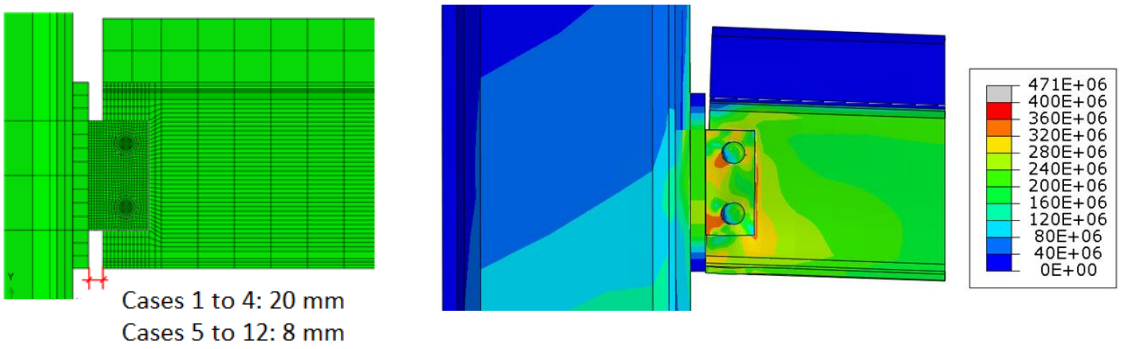

(a) (b)

Figure 12. Effects of gap distances (a) definition of gap distance for different cases (b) von-Mises stress contour at 68 minutes in Case 5.

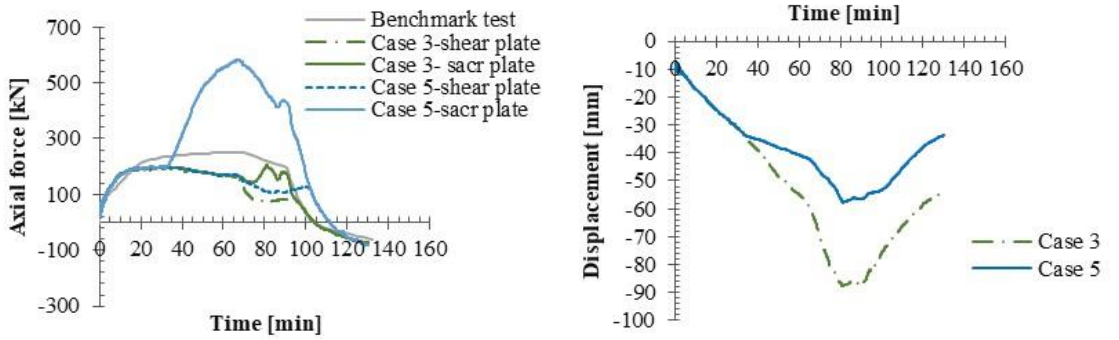

(a) (b)

Figure 13. Effects of gap distances on the development of axial forces and displacements in Case 3 (20 mm) and Case 5 (8 mm) (a) axial force (b) mid-span displacement.

Effects of thermal inputs

When the beams heated and cooled directly from the surfaces (Case 5) or indirectly by heat flux (Case 6), the axial forces in both beams (Figure 14 (a)) were similarly developed except in Stage I. Compared to the beam heated through surface, the beam heated by heat flux reached the maximum axial force in a slower rate. The contact between the beam and the sacrificial plate occurred at 44 minutes, which was about 10 min later. However, both beams reached the maximum compression force 600 kN at 70 minutes. As shown in the same figure, for the beam directly cooled at surfaces or indirectly by gas, the axial forces were developed similarly.

The observations can also be confirmed by the displacement response shown in Figure 14 (b). At the same maximum temperature, using the heat flux as a thermal input clearly reduced the displacement of the composite beam in Stage I. Both beams accelerated deflections at round 65 min till the cooling started. Because of the larger deflection reached, the beam cooled at surfaces recovered less. Both beams had the residual deflections of 25 mm to 35 mm. The results of axial forces and displacements also indicate that using either surface temperatures or heat flux as thermal input can well capture the responses of the studied beam. The heat flux as thermal input will be used for the further studies.

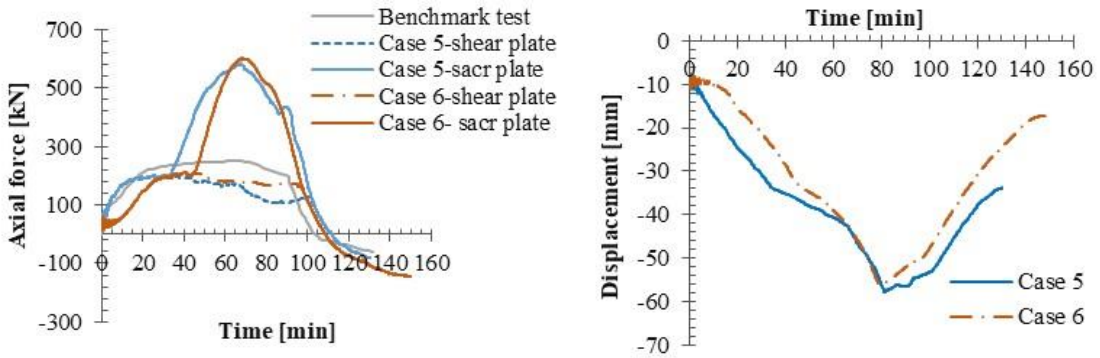

(a) (b)

Figure 14. Effects of surface temperatures (Case 5) or heat flux (Case 6) as thermal input on the beam responses (a) axial forces (b) displacements.

Effects of the locations of fire exposures

As shown in Figure 15 (a), the beams heated and cooled uniformly along the span (Case 6) or close to the connection (Case 7) behaved differently in terms of 4-stage mechanism. In the beam heated and cooled close to the connection, the axial forces increased gradually during the heating phase and decreased gradually during the cooling phase. No sudden changes were observed. In Stage II, the contact between the beam and the sacrificial plate occurred at 75 minutes. About 10 minutes later the gap was re-opened. Therefore, the compression axial forces increased less.

In the beam heated and cooled uniformly over the whole span, in Stage I, the axial force increased in a faster rate and reached the maximum axial force of 200 kN in the shear plate. The sudden change of the axial force in Stage II and sudden transition from compression to tension in Stage III were observed in the shear plate when the gap between the beam end and the column was closed and re-opened. The differences of axial forces between two beams in Stage I to Stage IV indicated that heating and cooling of the connection region locally was not so detrimental to the beam as the heating and cooling of the beam uniformly.

The similar results can be observed from the displacement. Figure 15 (b) shows that the maximum vertical deflection at mid-span in Stage I was about 25% less in the beam heated and cooled uniformly than that in the beam heated and cooled locally close to the connection. In Stages II and III the beam heated and cooled uniformly deflect in an accelerated rate and reached the maximum deflection of 50 mm, which is about 40 mm larger than the beam cooled close to connection. At the end of the cooling phase, the residual displacement in the beam cooled uniformly is around 18 mm, 8 mm more than that of the beam cooled close to the connections.

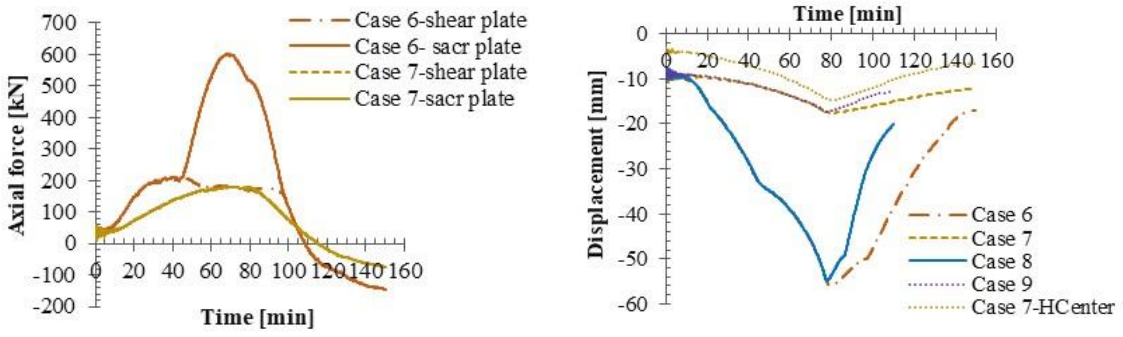

(a) (b)

Figure 15. Effect of heating and cooling the whole beam (Case 6) or close to connections (Case 7) on (a) axial force response (b) displacement response.

Effects of the cooling rates

In Case 8 and Case 9, the beams were heated as the beams in Case 6 and Case 7 but cooled faster. The developed axial forces are compared between Case 6 and Case 8 in Figure 16 (a) and between Case 7 and Case 9 in Figure 16 (b), respectively. For the beams with a higher cooling rate (Case 8 and Case 9), the closed gap was re-opened earlier, and the axial forces changed more suddenly from compression to tension. Although the beams cooled at different rates, the maximum tension force reached was

125 kN for Case 6 and Case 8, and 50 kN for Case 7 and Case 9, respectively. Similarly, the displacement responses shown in Figure 15 (b) show that the beams cooled faster (Case 8 and Case 9) recovered the displacements faster and had smaller residual displacements than the beams cooled slower (Case 6 and Case 7).

The maximum principal stresses of the shear plate at the end of the cooling phase are shown in Figure 17. Compared to the beam heated and cooled uniformly (Case 6), the beam heated and cooled close to the connections (Case 7) developed smaller tension stresses in the shear plate as the region of the highly tensioned region close to the welds is smaller. Under the developed axial load of 50 kN, the shear plate distorted slightly, and the principal tension stresses were smaller in the upper corner close to the welds.

Compared to the same beam (Case 6), the beam heated and cooled uniformly with a faster cooling rate (Case 8) also had a smaller high-tensile region close to the weld. The faster cooling led to a smaller yield zone in the shear plate compared to the case with the slow cooling. Under a similar axial load of 125 kN, the fast-cooled beam had the same level distortion and principal stresses at the upper corner close to the welds as in Case 6 (gray area with a yield strength of 400 N/mm^2).

As for the beam heated close to the connection and cooled faster (Case 9), the tension stresses developed in a much smaller region under the axial tension force of 50 kN. Because of the axial force changed more suddenly from compression to tension, the larger maximum principal tension stresses at the upper corner close to the welds were observed. The results indicate that the beam cooled close to the connections with a slower rate can delay the fracture of the shear plate close to the welds compared to the other studied cases. However, when the cooling rate was increased, the connections might be fractured under a lower axial force developed.

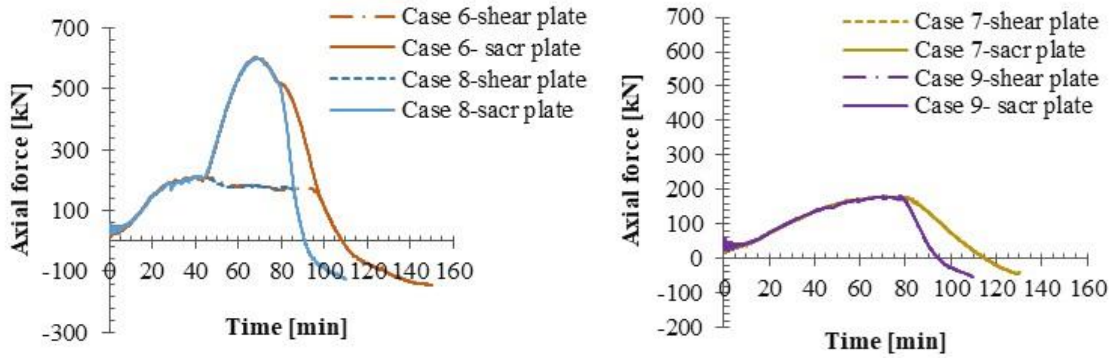

(a) (b)

Figure 16. Comparisons of axial forces developed in the sacrificing plate and shear plate at different cooling locations with different cooling rates (a) slower and faster cooling rate for the whole beam (Case 6 and Case 8) (b) slower and faster cooling rate for the region close to connection (Case 7 and Case 9).

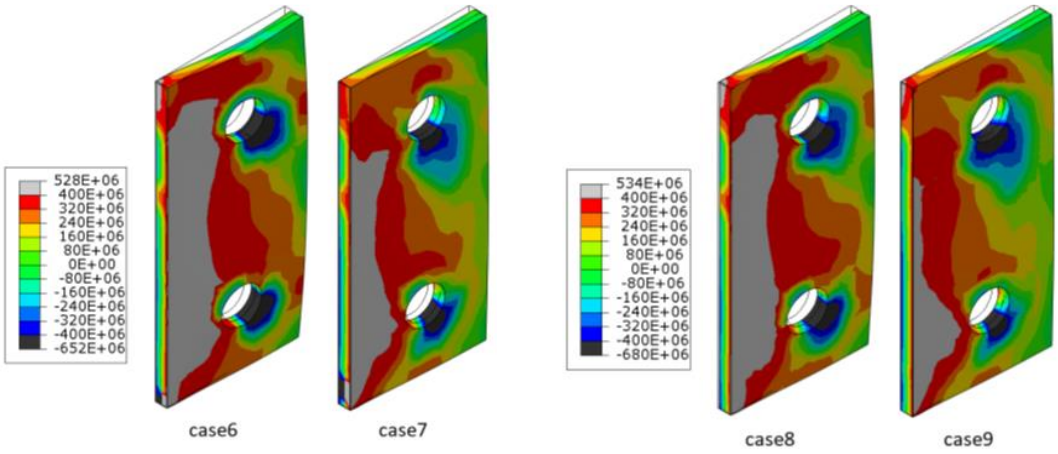

Figure 17. Maximum principal stresses output from the shear plate at the end of the cooling phase for Case 6 (whole beam), Case 7 (1 m close to connection), Case 8 (whole beam with faster cooling rate), and Case 9 (1 m close to connection faster cooling rate).

Effects of cooling region and cooling cycles

The FE models previously created were exposed to heating and cooling cycles (Case 10) shown in Figure 18 (a). The beam was heated to 700 ℃ in 15 min, followed by rapid cooling for 2 min, then heated again to 450 ℃ in 15 min, then cooled within 4 min back to room temperature. The total simulation time was 60 min. The heating-cooling cycles were designed as in [18] for simulating the beam exposed to travelling fire or fire interventions by water sprays.

Figure 18 (b) shows the temperature developed across the cross-section of the composite beam for Case 10. The development of the temperatures of the web, the bottom flange, and the exposed side of concrete slab trended similarly as the cyclic thermal inputs. However, the cooling of the top flange of the steel beam and the unexposed surfaces of the concrete slab were delayed. At the end of the 1st heating phase, a large thermal gradient was observed across the cross-section. The web reached the maximum temperature of 700℃ and the temperature reached in the top flange of the steel beam was about 200 ℃. During the 1st cooling phase, the temperature of the top flange slightly decreased. Instead of cooling, the temperature of the centre of the concrete and the unexposed concrete surfaces increased. At the end of the 2nd heating phase, the thermal gradient across the cross-section was still observed but was small. At the end of the 2nd cooling phase, the top flange reached its highest temperature whereas the web and the bottom flange have the lowest temperature. The temperature across the cross-section became more uniform.

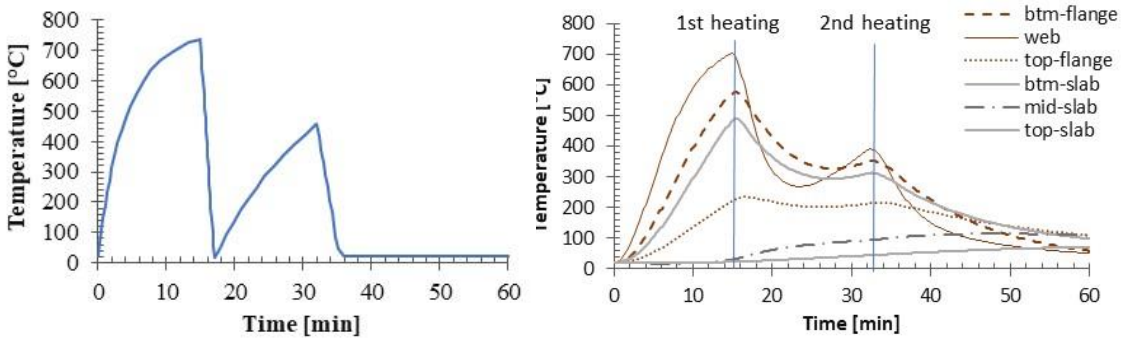

(a) (b)

Figure 18. Effects of heating and cooling cycles on the thermal response of the beam (a) cyclic thermal input (b) thermal response at different locations of the cross-section.

Figure 19 (a) shows the axial forces developed at the connection and the sacrificial plate during the cyclic heating and cooling. For all the studied cases, the 4-stage mechanism can be observed in each heating and cooling cycle. Among the three studied case, the axial forces were highest in Case 10 because the whole model was exposed to fire.

Compared to the beam in Case 10, the beam in Case 12 developed axial forces in a slower rate during the heating stage due to the lower stiffness of the support provided by the unheated beam. Before the 1st cooling phase started, the hinge mechanism was not activated. The rotation of the beam was small; therefore, the gap was closed for a noticeably brief time. During the cooling phase, compressive axial forces dropped. During the 2nd heating and cooling cycle, the axial force changed from compression to tension. However, the magnitude of the cyclic load was not as large as in Case 10.

Among three studied cases, the axial forces developed was lowest when the beam was heated close to the connection (Case 11). During the first heating and cooling cycle, the unexposed part of the beam was longest, thus leading to the lowest stiffness to restrain the thermal expansion. The beam did not rotate enough to close the gap to the sacrificial plate, therefore, axial forces in the shear plate and sacrificial plate matched. During the 2nd heating and cooling cycle, the axial force changed from compression to tension, and the magnitude of the cyclic load was close to that in Case 12.

For all the studied cases, the vertical displacement at midspan agreed well with the response of the axial forces as shown in Figure 19 (b). At the end of the 1st heating phase, the maximum displacement was 86 mm (Case 10), which is less than the deflection limit of L/20 (225 mm). When the cooling phase started, the deflection of the beam recovered. As the 2nd heating phase started, the displacement increased again. At the end of the cooling stage, the deflection of the beam recovered but not to the original deflection. The results indicate that the heating and cooling of the beam close to the connection developed less axial force and residual deflection.

Figure 20 (a) to (e) show the change of maximum principal stresses close to the end of both 1st and 2nd cooling cycles for Case 10. At the end of the 1st cooling cycle, the tension axial forces were observed in the upper corner of the shear plate close to the welds (Figure 20 (b)). The axial force developed in the shear plate was the same as that

developed in the sacrificial plate. At the end of the 2nd cooling cycle, the tension forces were developed in a large part of the shear plate close to the welds. It seems that the failure can have been initiated at the end of the 1st cooling phase, but the actual failure occurred in the 2nd cooling phase.

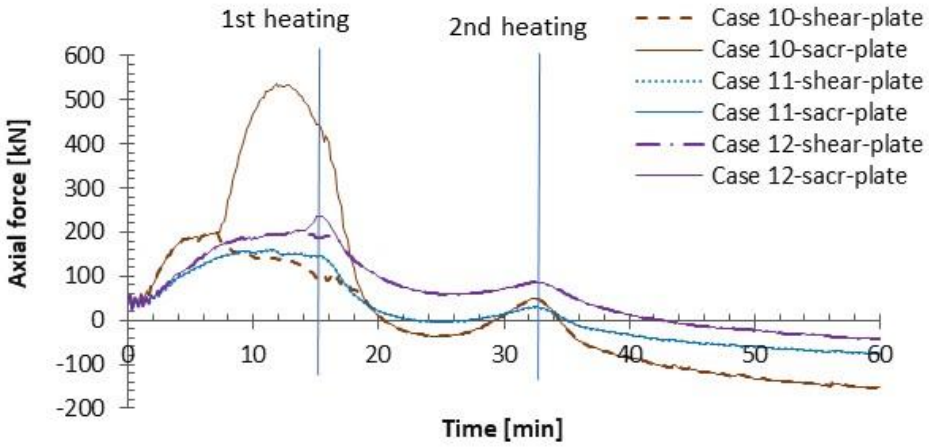

(a)

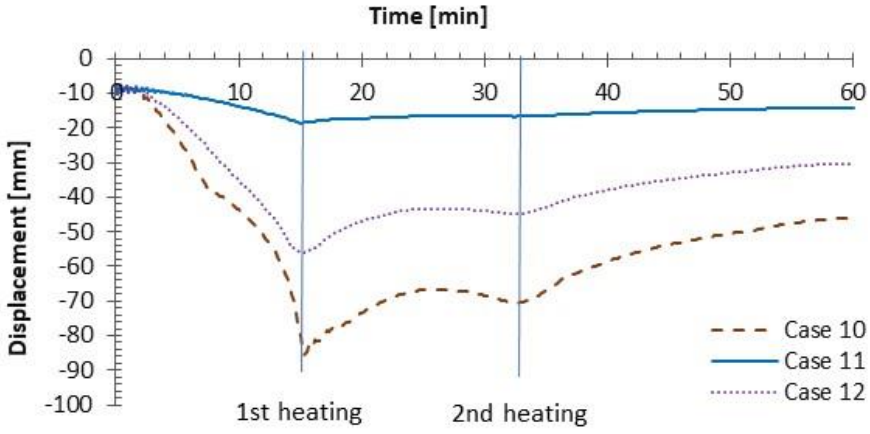

(b)

Figure 19. Structural responses of the beam exposed to heating-cooling cycles for Case 10 to Case 12 (a) axial forces developed at sacrificial plate and shear plate (b) mid-span displacement.

Figure 21 (a) to (c) show the maximum principal stresses output from the shear plate at the end of 2nd cooling stage for Case 10 to Case 12. For Case 10, extremely high area of tension stresses along the welding line and exceedingly high area of compression stresses around the bolt holes are observed. In Case 11, when the beam was heated close to connections, high-tension stresses were observed near the weld line. Therefore, the fracture failure can be expected at the weld line. In Case 12, tensile stresses were smaller in the upper corner close to the welds. Therefore, the fracture failure may not occur in the shear plate.

For all the studied cases, the shear stud connectors behaved similarly in the Stage I, Stage II, and Stage IV except in Stage III. Temperatures reached in Stage III degraded the material properties differently, thus activating the slip of the shear stud at different levels. The higher temperatures at the top flange generated larger slips. The maximum slip occurred in Case 3 and was less than 6 mm. According to the failure criteria for the shear connectors defined previously, it can be concluded that all the connectors functioned well.

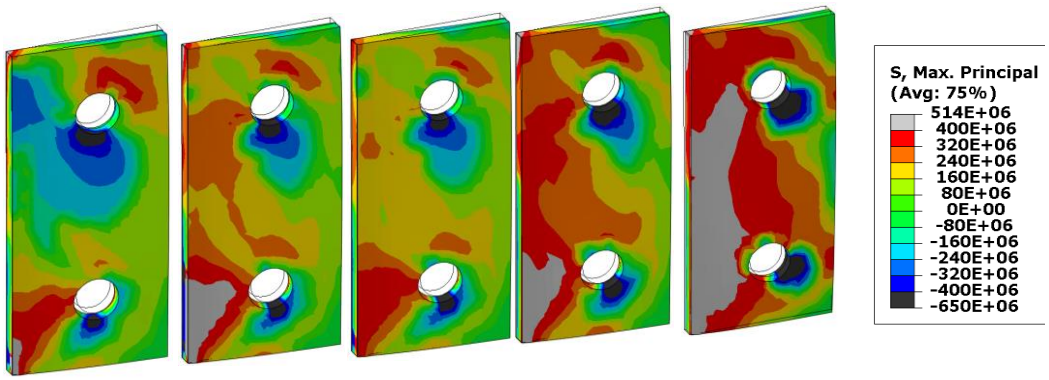

(a) 20 min (b) 25 min (c) 28 min (d) 37 min (e) 60 min

Figure 20. Development of maximum principal stresses inside shear plate for Case 10.

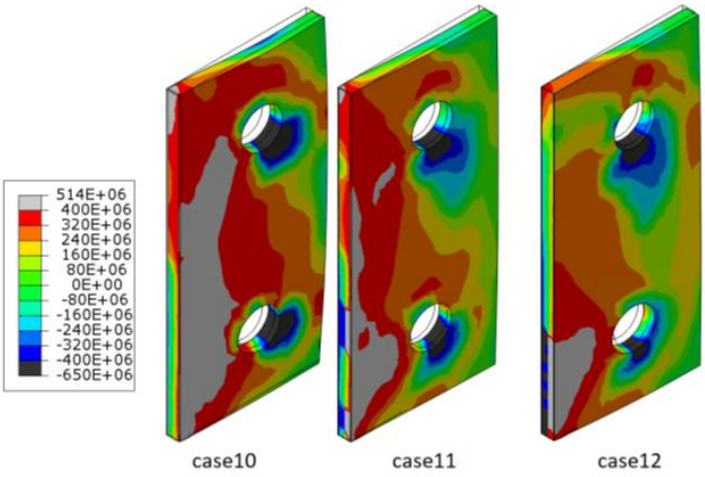

Figure 21. Maximum principal stresses output from the shear plate in the end of the cooling phase for Case 10 (uniformly heating and cooling), Case 11 (1 m close to connections) and Case 12 (1 m close to mid-span)

Conclusions

In this research, the behavior of the shear plate connection fixing a composite beam to columns was studied using finite element analyses. The FE models were validated by the test results and further used to study the load-bearing mechanism of composite beams exposed to fires. Parametric studies were conducted to study the effect of a clearance between the beam flange and the column, the effect of fast cooling, and

heating and cooling cycles for the whole model, the 1 m long part of the beam near the beam and column connection, and 1 m long part of the beam at the middle of the -span.

FE models well simulated the behaviour of the shear plate connection at elevated temperatures. During the heating phases, the strength of the connection did not exceed the shear strength of the bolts. During the cooling phase, the shear plate fractured along the welding line in the tests. In FE models, the actual welds were modelled using the tie constraints, thus restricting the actual occurrence of the fracture. The fracture was defined as when the maximum principal stress in the shear plate exceeds the yield strength of the steel.

The closure of the gaps can change a hinge connection to a moment connection at elevated temperatures. The higher axial restraint can be induced by the gap closure. The beam deflections were reduced, thus delaying the transition from axial compression to axial tension and leading to smaller residual deflections during the cooling phase. Compared to the fast cooling of the beam close to its connections, the slow cooling at the same location was not so detrimental. The axial force developed gradually, and the beam deflected less. The fin-plate connection had a smaller overstressed region at the upper corner close to the welds. During the heating and cooling cycles, the axial forces developed at beam ends were fluctuating from compression to tension and vice versa. The weakest part of the connections was the shear plate because of the highest stresses and lower material strength. At the end of the first cooling phase, larger tension forces developed close to the welds predicted the initial fracture of the welds. At the end of the second cooling phase, these higher tension forces predicted the fracture failure at the same location.

Based on the research results, some recommendations for practical design can be given. The change of a fin-plate connection from a pined to a moment connection at elevated temperatures benefits the behaviour of composite beams if the clearance is properly defined and the connections are deliberately detailed. To ensure the development of the catenary action in the beam before the final collapse, cooling the connections in a faster rate should be avoided, and the cooling location is recommended to be away from the connection region. In the connections exposed to cyclic heating and cooling, fracture failure often initiates in welds during the first heating and cooling cycles. Therefore, it is recommended to dimension welds considering the maximum tensile axial force reached during these cycles. Studying the behaviour of a simple shear connection exposed to other fire scenarios will show more insights about the failure of the connection during the cooling phase. A better understanding of the behaviour of the connection will improve the design and detailing for fire resistance in steel-framed buildings.

Acknowledgement

The research was carried out at Aalto university with the collaboration of Tallinn University of Technology for finishing Master's Thesis of the first author. The visit for exchange studies and doing thesis research is financially supported by the European Union, namely the Erasmus Scholarship.

References

[1] G. Brambilla, M. Lavagna, G. Vasdravellis and C. A. Castiglioni. Environmental benefits arising from demountable steel-concrete composite floor systems in buildings. Conservation and Recycling, 141:133–142, 2019. https://doi.org/10.1016/j.resconrec.2018.10.014

[2] N. Alam, A. Nadjai, M. Charlier, O. Vassart, S. Welch, J. Sjöström, X. Dai. Large scale travelling fire tests with open ventilation conditions and their effect on the surrounding steel structure– The second fire test. Journal of Constructional Steel Research, 107032, 2022. https://doi.org/10.1016/j.jcsr.2021.107032

[3] V.R. Ramsamy, E. Annerel, K. Van Masele, G. Maragkos, B. Merci. Analysis of travelling fires and comparison to the travelling fire methodology. SFPE Europe, vol. 20, 2020. https://www.sfpe.org/publications/periodicals/sfpeeuropedigital/sfpeeurope20/europeissue20feature3

[4] E. Rackauskaite, P. Kotsovinos, A. Jeffers, G. Rein. Structural analysis of multi-storey steel frames exposed to travelling fires and traditional design fires. Engineering Structures, 150:271–287, 2017. https://doi.org/10.1016/j.engstruct.2017.06.055

[5] S. Shakil, W. Lu, J. Puttonen. Behaviour of vertically loaded steel beams under a travelling fire. Structures, 44:1–17, 2022. https://doi.org/10.1016/j.istruc.2022.07.084

[6] R.K. Janrdhan, S. Shakil, W. Lu, S. Hostikka, J. Puttonen. Couplded CFD-FE analysis of a long-span truss beam exposed to spreading fires. Engineering Structures, 114150, 2022. https://doi.org/10.1016/j.engstruct.2022.114150

[7] R.K, Janardhan, S. Shakil, M. Hassinen, W. Lu, J. Puttonen, S. Hostikka. Impact of firefighting sprays on the fire performance of structural steel members. Fire Technology, 2022. https://doi.org/10.1007/s10694-022-01257-8

[8] B. Zhao and J. Kruppa. Fire resistance of composite slabs with profiled steel sheet and of composite steel concrete beams, part 2: composite beams. Luxembourg: European Commission, 1997. https://op.europa.eu/en/publication-detail/-/publication/10f40312-b040-4fda-bc0a-ab657f6a3e41

[9] E.C. Fischer and A.H. Varma. Fire behavior of composite beams with simple connections: benchmarking of numerical models. Journal of Constructional Steel Research, 111:112–125, 2015. https://doi.org/10.1016/j.jcsr.2015.03.013

[10] S. Kristi. Experimental investigation of composite beams with shear connections subjected to fire loading. Journal of Structural Engineering, 142(2), 2015. https://doi.org/10.1061/(ASCE)ST.1943-541X.0001

[11] E.C. Fischer, S.L. Kristi and A.H. Varma. Experimental evaluation of the fire performance of simple connections. Journal of Structural Engineering, vol. 143(2), 2016. https://doi.org/10.1061/(ASCE)ST.1943-541X.00016

[12] L. Choe, S. Ramesh, W. Grosshandler, M. Hoehler, M. Seif, J. Gross, M. Bundy. Behavior and limit states of long-span composite floor beams with simple shear connections subject to compartment fires: experimental evaluation. Journal of Structural Engineering, 146(6), 2020. https://doi.org/10.1061/(ASCE)ST.1943-541X.00026

[13] B. 476, Fire tests on building materials and structures. Part 20. Method of determination of fire resistance of elements of constructions. British Standard Institution, 1987.
[14] Abaqus 6.13 Analysis user guide, Providence, RI, USA: Dassault Systèmes, 2013.
[15] EN 1993-1-2, Design of steel structures – Part 1-2: General rules – Structural fire design. CEN, Brussels, 2005.
[16] EN 1992-1-2, Eurocode 2: Design of concrete structures – Part 1-2: General rules – Structural fire design, 2004.
[17] Z. Abebe, S. Shakil, W. Lu, J. Puttonen. Post-fire mechanical properties of steel S900MC, in EUROSTEEL 2021, Sheffield, U.K., 2021. https://doi.org/10.1002/cepa.1467
[18] A. Hoang. Effect of non-uniform temperature field on the behaviour of a steel member exposed to fire, Master thesis, Aalto University, Espoo, Finland, 2020.

Mohamed Sakr, Wei Lu, Jari Puttonen
Department of Civil Engineering
Aalto University
mohamed.anas.970@outlook.com, wei.2.lu@aalto.fi, jari.puttonen@aalto.fi

Mohamed Sakr, Ivar Talvik
Department of Civil Engineering and Architecture
Tallinn University of Technology, Estonia
ivar.talvik@taltech.ee